Graphene Nanoribbon Devices Produced by Oxidative Unzipping of Carbon Nanotubes

Alexander Sinitskii,[†] Ayrat Dimiev,[†] Dmitry V. Kosynkin,[†] and James M. Tour[†,‡,*]

[†]Department of Chemistry and [‡]Departments of Computer Science, Mechanical Engineering and Materials Science, and the Smalley Institute for Nanoscale Science and Technology, Rice University, MS 222, 6100 Main Street, Houston, Texas 77005

ABSTRACT We demonstrate that graphene nanoribbons (GNRs), produced by the chemical unzipping of carbon nanotubes, can be conveniently used from solution to hand-paint unidirectional arrays of GNRs atop silicon oxide. Through this simple alignment technique, numerous GNR-based devices, including field effect transistors, sensors, and memories can be easily fabricated on a single chip, and then used to generate statistically relevant device assessments. Such studies immediately give insights into, for example, multilayering properties on conductance, the profound effects that atmospheric adsorbates have upon the transfer characteristics of graphene, and other phenomena affecting the performance of GNR devices.

KEYWORDS: graphene · graphene nanoribbons · carbon nanotubes · field-effect transistors · nonvolatile memories.

Graphene is a two-dimensional carbon material that has attracted intense interest due to its remarkable electrical properties.[1−11] Chemical vapor deposition (CVD) growth of large-area mono- and bilayer graphene sheets is rapidly improving,[12,13] and it will likely be the preferred route, coupled with lithography, to generate very large-scale integrated devices of the future. However, presently most graphene device properties are painstakingly assessed using exfoliated graphene flakes. These flakes require micro- and nanoscopic characterization and processing, and statistically significant measurements are only laboriously obtained. In this paper we demonstrate that recently discovered graphene nanoribbons (GNRs),[14] produced by the chemical unzipping of carbon nanotubes, can be conveniently used from solution to hand-paint unidirectional arrays of GNRs atop silicon oxide. We show that with a simple alignment technique, numerous graphene-based field-effect transistors (FETs), sensors or memories can be easily fabricated on a single chip, and statistically important device behaviors can be rapidly recorded. These devices were recently shown to be useful in studies ranging from GNR electrical measurements[15] and investigation of their chemical reactivity with diazonium salts,[16] to the probing of the morphology of the GNR corrugation atop SiO_2.[17]

Several different approaches have been used to fabricate GNRs, including lithography,[8,9,18] masking graphene with inorganic nanowires,[19,20] a sonochemical method,[21] a bottom-up approach,[22] and unzipping of carbon nanotubes.[14,23−27] For this study we used the graphene oxide (GO) nanoribbons (GONRs) obtained by the oxidative unzipping of multiwalled carbon nanotubes (MWCNTs) in a sulfuric acid solution of potassium permanganate, as reported in our previous work.[14] These ribbons benefit from simple, bulk, scalable fabrication with nearly 100% yield, which makes them an interesting and promising object to study, although, as we show below, the GNRs produced by reduction of GONRs have electrical properties inferior to those of the GNRs produced by approaches that do not involve oxidative chemistry.

The GONRs have a structure similar to that of GO: a multifunctional organic network containing mostly epoxy and hydroxyl functionalities on basal planes with carbonyl and carboxyl groups at the edges. As-prepared GONRs are poor conductors,[14] similar to GO flakes prepared by conventional methods.[28−34] The MWCNTs have starting diameters of 40−100 nm and up to ~30 nanotube layers; hence, once unzipped, they produced stacks of multiple GONRs. These stacks of GONRs are prone to aggregation, and despite the numerous functionalities they bear, they could not be dispersed as few-layered structures in deionized (DI) water. Thus the GONRs were treated with hydrazine, which has previously been shown to be an effective agent

*Address correspondence to tour@rice.edu.

Received for review May 10, 2010 and accepted August 19, 2010.

Published online September 2, 2010.
10.1021/nn101019h

for the deoxygenation of GO and increasing its conductivity.[29−34] In a typical procedure, GONRs were dissolved in aqueous ammonia at pH 9−10, thus producing a brown dispersion. Further addition of hydrazine turns the dispersion black due to the formation of extended aromatic domains in the exfoliated nanoribbons. Interestingly, the hydrazine treatment not only reduces the nanoribbons and helps to disperse them in aqueous media, but it also facilitates their exfoliation from thick stacks to mono- or few-layered GNRs. The easier exfoliation may be explained by partial removal of hydroxyl groups responsible for strong hydrogen bonding between neighboring GONR layers by hydrazine reduction. However, near-complete reduction results in the increased interaction between graphene layers, forming a graphite-like structure. Therefore, to produce the minimum interaction between the individual graphene layers within the stacks, thus enabling their separation, the "almost-reduced" GNRs, with small amounts of remaining oxygen-containing groups acting as spacers between graphene layers, are the preferred product. Indeed, the highest concentration of mono- and bilayer reduced GNRs can be achieved after 40−50 min of the hydrazine treatment at 85 °C and subsequent gentle bath ultrasonication for 1 min (the more intense cup-horn or probe sonication will cut the nanoribbons). A smaller fraction of thin GNRs was found in the solutions treated with hydrazine for longer times. Reduction for more than 2 h caused complete aggregation of the colloidal mixture.

The GNRs were deposited onto Si/SiO_2 substrates for further studies. Two different approaches were employed for the deposition. Samples with uniform thick (>0.1 μm) coatings of densely packed GNRs for the Raman and X-ray photoelectron spectroscopy (XPS) studies were prepared by casting concentrated solutions of GNRs onto the substrates and removing the solvent. For the device fabrication, isolated individual or thin-layered GNRs were desired, and another approach was developed for their deposition. A droplet of a dilute solution of GNRs was put onto the substrate and spread over it by repeated unidirectional (*i.e.*, repeated "north-only" as opposed to "north−south") strokes with a soft paintbrush while the surface was permitted to dry (see the inset in Figure 1a). The paintbrush-induced shear forces upon the long and thin structures produced directional alignment of the GNRs. After drying, the substrate was washed by a stream of DI water directed in the same direction as that used for the brushing. The van der Waals interaction of the GNRs with the SiO_2 surface was strong enough to retain the nanoribbons on the substrates.

SEM studies suggest that after 40−50 min of the hydrazine treatment, a significant proportion of GNRs could be found as mono- or bilayer nanoribbons; typically 3−10% were monolayer and 3−10% were bilayer nanoribbons of the total number analyzed in a given substrate area. The remainders are either multilayer GNRs or elongated aggregates of several GNRs with a total width of up to 1 μm and length of up to 20 μm. Most of the tracked monolayer GNRs had widths of *ca.* 180−320 nm. The simple brushing technique induced the alignment of the GNRs on the substrate, as shown in Figure 1a, where the majority of the GNRs and stacks have the same orientation. Individual mono- and bilayer GNRs cannot be seen at such low magnification, but for them we have observed a similar alignment effect as well. Such alignment of the GNRs is very useful for the device fabrication, since only orthogonal lithographic patterns of electrodes are required for making a large number of devices. Interestingly, other approaches producing a sufficient shear force also enable an alignment of GNRs. For instance, Figure 1b shows a sample that was prepared by blowing a droplet of GNR solution over a Si/SiO_2 substrate with a strong flow of nitrogen. Alignment of the GNRs, similar to the case of paint-brushing, is clearly seen. We anticipate that other conventional approaches such as electrophoresis could also be used for the alignment of GNRs.

We have compared SEM and AFM images for >30 GNRs and found that it is possible to distinguish mono-, bi-, and multilayer GNRs simply by their appearance in the SEM images. Monolayer GNRs are half-transparent to the electron beam, so that their brightness is very close to that of a substrate; any rare foreign objects, such as microscratches and nanoparticles, are clearly visible through the nanoribbons. Most importantly, monolayered GNRs have their long edges parallel to each other. These properties of monolayer GNRs are illustrated by Figure 1c−g. The difference in appearance of mono- and bilayer GNRs is demonstrated in Figure 1 panels h and i, which show the GNRs with coexisting mono- and bilayer fragments. Bilayer GNRs appear darker in the SEM images though they are still partially transparent. Importantly, the top and bottom layers of bilayer GNRs never perfectly coincide since they originate from different shells of MWCNTs. Therefore, monolayer portions are always observed in the SEM images of bilayer GNRs, which ensures their reliable identification; this is illustrated by Figure 1j,k. After initial AFM correlation, mono- and bilayer GNRs can be identified by routine SEM; no laborious AFM measurements are required for the height analysis, thereby streamlining device fabrication. It is difficult to estimate the thickness of the stacks of GNRs with more than three graphene layers, appearing in the SEM images as dark nontransparent strips with randomly shaped edges (Figure 1l); they were not considered for electrical measurements. Figure 1 panels m and n show the images of a fragment of the same monolayer GNR, obtained by SEM and AFM, respectively; such pairs of images obtained for different mono-, bi-, and multilayer GNRs were used to identify the above features. After 40 min of hydrazine

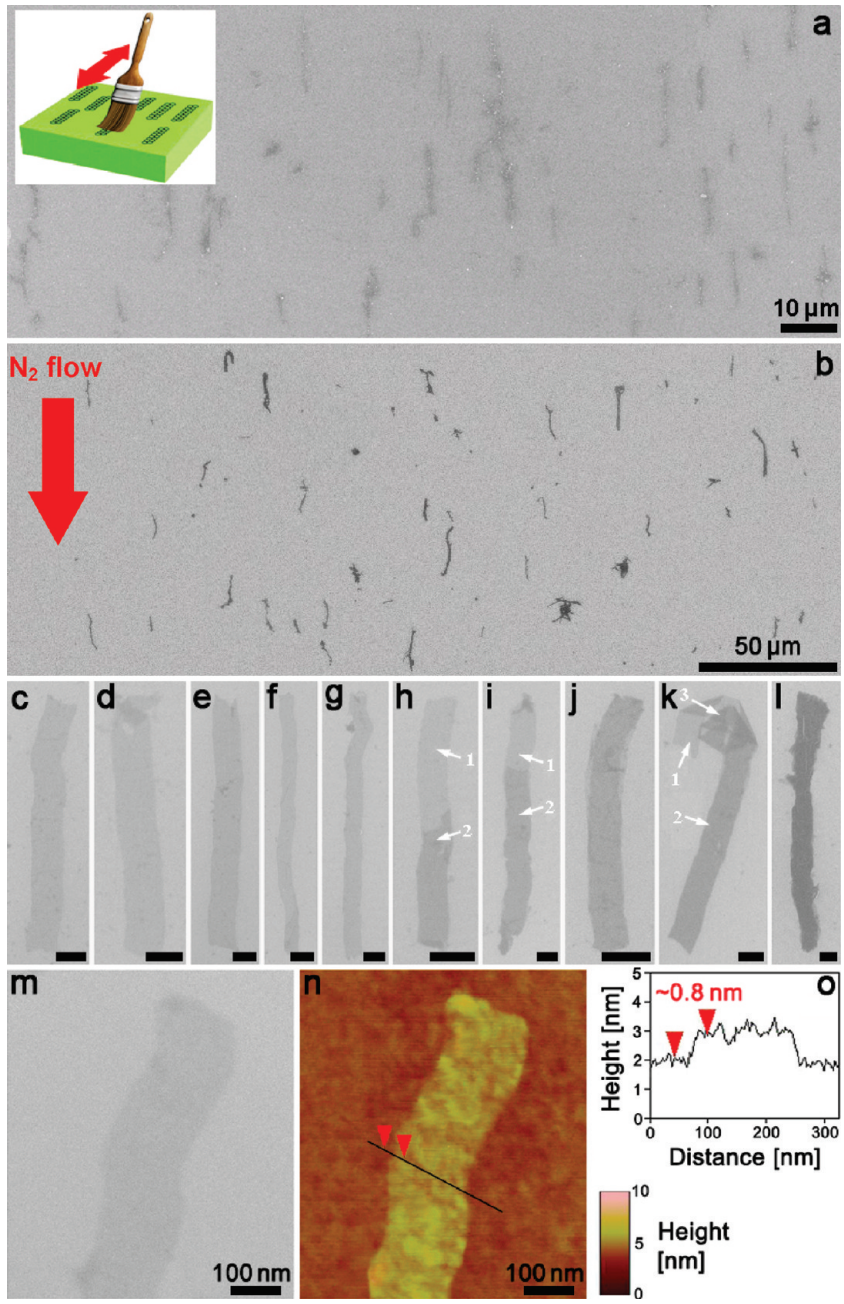

Figure 1. Images of the hydrazine-reduced GNRs deposited on a Si/SiO_2 substrate. Low-magnification SEM images of the GNRs aligned by the paint-brushing technique (a) and by blowing a droplet of GNR solution over a substrate with a strong flow of nitrogen (b). The alignment of the GNRs in panel a was achieved by simple paint-brushing strokes during drying, as schematically shown in the inset in panel a; red arrow in panel b shows the direction of the N_2 flow. Magnified SEM images of monolayer nanoribbons (c−g), GNRs with coexisting mono- and bilayer fragments (h,i), bilayer nanoribbons (j,k), and a multilayer stack of GNRs (l). All GNRs in panels c−l had the same orientation on a Si/SiO_2 substrate; the images were not rotated for this Figure. Arrows in panels h, i, and k show the number of layers in the corresponding areas of the GNRs; the region in panel k with effective trilayers arises due to the folding of the upper layer in a bilayer GNR. Scale-bars for panels c−l are 250 nm, except for panel f at 500 nm. All GNRs in panels c−k have a width of 180−320 nm, they can be up to several μm long, as shown in panels f at 6.1 μm and g at 3.2 μm. (m,n) Images of a fragment of the same monolayer GNR, obtained by SEM and AFM, respectively. (o) Height profile measured along the black line in panel n.

reduction, the monolayer nanoribbons typically had a thickness of 0.7−1.1 nm (Figure 1o), whereas bi- and trilayer GNRs were proportionally thicker. The determination of the exact number of layers in the thick stacks of GNRs by AFM was also challenging due to the uncertainty of the thickness of a single-layer nanoribbon. Despite the convenience of using SEM for the identification of the number of layers in the GNR stacks, such analysis prior to the device fabrication should be done carefully, without using high acceleration voltages and unjustifiably long exposures, because a recent micro-Raman spectroscopy study revealed that extensive electron-beam irradiation results in damage to the graphene.[35]

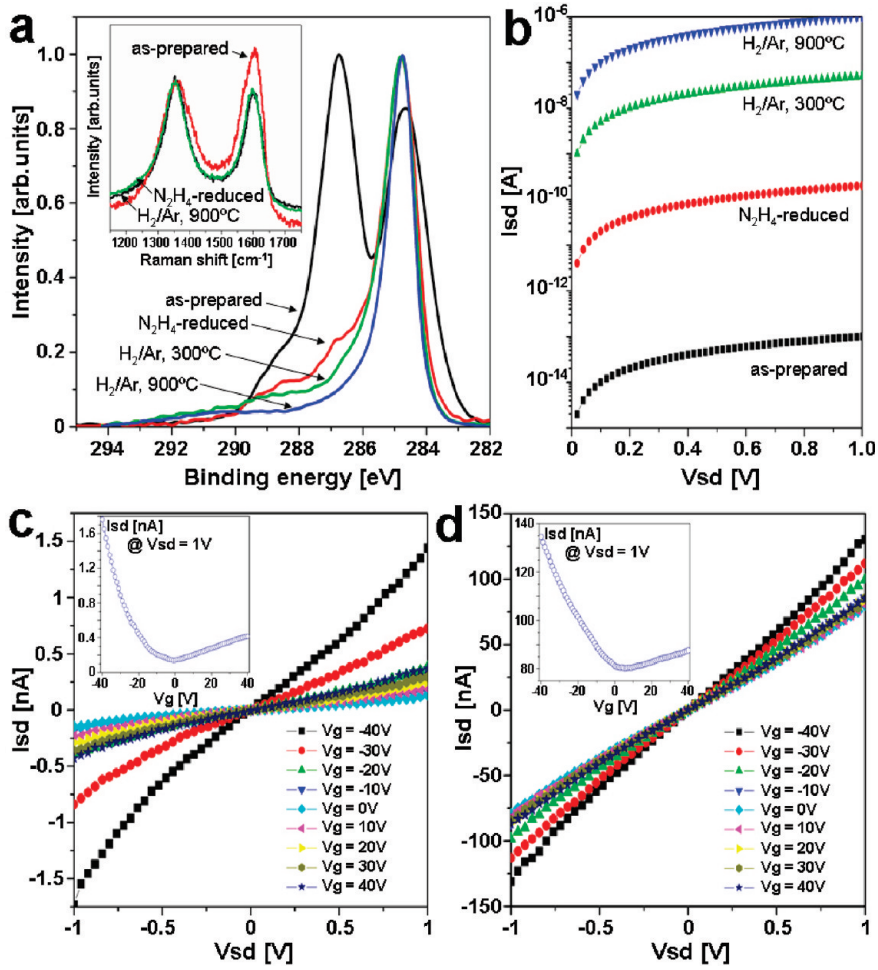

Figure 2. Reduction of GONRs and electrical testing. (a) C1s XPS and Raman (inset) spectra and (b) logarithmic IV curves for the nanoribbons with different degree of reduction. (c,d) Source-drain current (I_{sd}), source-drain voltage (V_{ds}) and gate voltage (V_g) dependencies (p-doped silicon was used as a back gate) for the same device based on a N_2H_4-reduced monolayer GNRs before (c) and after (d) annealing in H_2/Ar at 300 °C for 30 min. The transfer characteristics in the insets were recorded at the pressure of 10^{-5} Torr after <1 h of evacuation; see below for details.

Since GO is known to have poor conductivity, we used different approaches for the reduction of GONRs. In addition to the 40−50 min hydrazine treatment (as we noted, the largest fraction of mono- and bilayer GNRs was produced at that duration of treatment, though a higher degree of reduction could be possibly obtained by longer hydrazine treatment), we have also employed annealing in Ar/H_2 atmosphere at different temperatures. The C1s XPS spectra show the decrease in the amount of oxygen-containing functionalities in the GONRs upon reduction (Figure 2a). The peak at 284.8 eV corresponds to the C−C bond, whereas the overlapping peaks at 286−289 eV correspond to the carbon in different oxygen-containing functional groups. As expected, these peaks are still seen after 40−50 min reduction with hydrazine, though their intensity decreased dramatically. After annealing the reduced nanoribbons in Ar/H_2 at 300 °C for 30 min, the peak at 286.8 eV (C−O bonds) diminishes, and only a small shoulder at 288.8 eV is still observed, which probably corresponds to the edge carboxylic acid moieties. After annealing the same nanoribbons in Ar/H_2 at 900 °C for 1 h, the C−C peak at 284.8 eV is the nearly exclusive remaining feature.

The inset in Figure 2a shows the evolution of the Raman spectra of the nanoribbons upon reduction. GONRs, containing abundant oxygen functionalities, exhibit a D band at 1363 cm^{-1} and G band at 1594 cm^{-1} with comparable intensities. After reduction the I(D)/I(G) ratio slightly increases, a tendency that was previously reported for the reduced product of GO.[29] This is not particularly surprising, considering that sp^2/sp^3 ratio is not the only factor that determines the I(D)/I(G) ratio in carbon materials, and the latter may either decrease or increase with increasing sp^2 content, depending on the initial size and distribution of sp^2 domains.[36] For example, such effects of the sp^2 content on the I(D)/I(G) ratio was observed in the Raman studies of electron-beam-irradiated graphene.[35] Monolayer graphene obtained by micromechanical exfoliation exhibited no D band. The irradiation resulted in the decreasing crystalline quality of graphene and appearance of a pronounced D band, but further amorphization of graphene upon continuous irradiation was accompa-

nied by a decreasing *I*(D)/*I*(G) ratio.[35] In our case the increasing *I*(D)/*I*(G) ratio upon the reduction of GONRs to GNRs suggests that the average size of sp^2 domains in GONRs is very small. This conclusion seems to be reasonable, considering the harsh oxidative conditions in which GONRs are produced, and also the fact that even in the reduced GO materials the sp^2 domains are also typically considered to be on the order of a few nanometers.[31] Another factor affecting the *I*(D)/*I*(G) ratio in the Raman spectra of GO materials, is the possible presence of nanoscopic holes in the basal planes of GO and GONRs caused by the oxidative treatment of graphite or MWCNTs, respectively. It was demonstrated by micro-Raman spectroscopy that even graphene flakes prepared by micromechanical cleavage can exhibit a pronounced D band due to the edge effect.[37,38] Obviously, for GO material with nanoscopic holes, such edge effects would remain even after reduction since the holes would still exist.

All of the reduction conditions resulted in increased conductivity of the GNRs. Individual GNRs, mostly with mono- or bilayers, aligned on a silicon wafer (heavily doped p-type Si with 200 nm thermal SiO_2 layer), had Pt electrodes fabricated on top of them by standard e-beam lithography wherein the electrodes were deposited orthogonal to the paintbrush stroke direction. In a typical device, a GNR bridged two electrodes separated by 350−400 nm and the p^{++}-Si was used as a back gate. Exploiting the ease of device fabrication using MWCNT-unzipped GNRs, >300 of these two-terminal devices were obtained and the device statistics recorded. Figure 2b shows IV curves for the devices based on monolayer GNRs with different degrees of reduction; each curve is the average of ≥20 similar devices. The increase in conductivity after each reduction step is further illustrated by Figure 2 panels c and d, which display the electrical properties for the same device based on a N_2H_4-reduced monolayer nanoribbon before (Figure 2c) and after (Figure 2d) annealing in H_2/Ar at 300 °C for 30 min. The electrical properties of the annealed devices were qualitatively the same though their conductivity increased by 10−100-fold after annealing.

To determine the highest conductivity of the GNRs, we fabricated four-terminal devices based on mono-, bi-, and trilayer GNRs annealed in H_2/Ar at 900 °C for 1 h (see the schematic in Figure 3a). In such a configuration we could employ the four-probe method to eliminate the contact resistance effect and also study the field-effect by using the p-doped Si as a back gate. The SEM image of a typical device based on a monolayer GNR is shown in Figure 3b. Figure 3c shows the results of the four-probe measurements for a typical device based on a monolayer GNR. The device exhibits an ambipolar field effect typical for graphene.[1−3] We have observed the same qualitative behavior for the devices based on bilayer GNRs, though their conductivity was significantly higher. The comparison of the conductivities of mono-, bi-, and trilayer GNRs is shown in Figure 3d. At least 20 nanoribbons of each group were tested. We have found that the average conductivity of the reduced monolayer GNRs is 35 S/cm, which is significantly higher than 0.02−2 S/cm reported for reduced GO.[31] This result is surprising, considering the fact that both these GNRs and the reduced GO sheets are obtained by similar oxidative chemistries. However, it could be possibly explained by the fact that hydrogen plasma instead of high-temperature annealing was used in the work of ref 31 to achieve the highest degree of reduction. We have also found that bilayer nanoribbons are, on average, >2× more conductive than monolayer nanoribbons, featuring an average conductivity of ∼115 S/cm. This large difference in conductivity between mono- and bilayers was previously reported for the exfoliated graphene and reduced GO sheets,[31] and was attributed to the strong interaction between the bottom layer and the SiO_2 substrate.[10,31,39,40] Interestingly, the addition of the third layer also does not result in a linear increase in conductivity; trilayer GNRs exhibit an average conductivity of ∼210 S/cm, which suggests that the conduction of the top layer in a bilayer nanoribbon is also somewhat suppressed. This can be rationalized, in part, by the fact that the top and bottom layers of bilayer GNRs never perfectly coincide since they originate from different shells of MWCNTs, and therefore a significant part of the top layer is also in contact with the substrate. This effect is illustrated by Figure 3e,f. Figure 3e shows the SEM image of the electronic device based on hydrazine-reduced bilayer GNR. Figure 3f shows the same image, where the long edges of the different layers of the GNR are conveniently shown by red and yellow dashed lines (note that for each layer the long edges are nearly parallel). From this SEM image it is impossible to conclude which of two layers is the top and which is the bottom. However, whichever layer is on top, it has a significant portion in contact with the Si/SiO_2, for which the conductivity should be suppressed due to the interaction with the substrate.

Interestingly, we discovered that the appearance of the transfer characteristics strongly depends on the duration of the evacuation time in the probe station.[33,41] This effect is illustrated in Figure 3g where several transfer characteristic curves for the same monolayer nanoribbon device are plotted as a function of the evacuation time at 10^{-5} Torr. The first measurement (black squares in Figure 3g) was performed a few minutes after the evacuation was started, showing that the GNR is a p-type semiconductor. However, as the evacuation continued, the device started exhibiting an ambipolar field effect, as the hole conductivity decreased and electron conductivity increased. After 12 h of evacuation, the hole conductivity was still higher than the electron conductivity, but as the trend continued for 2 d, the

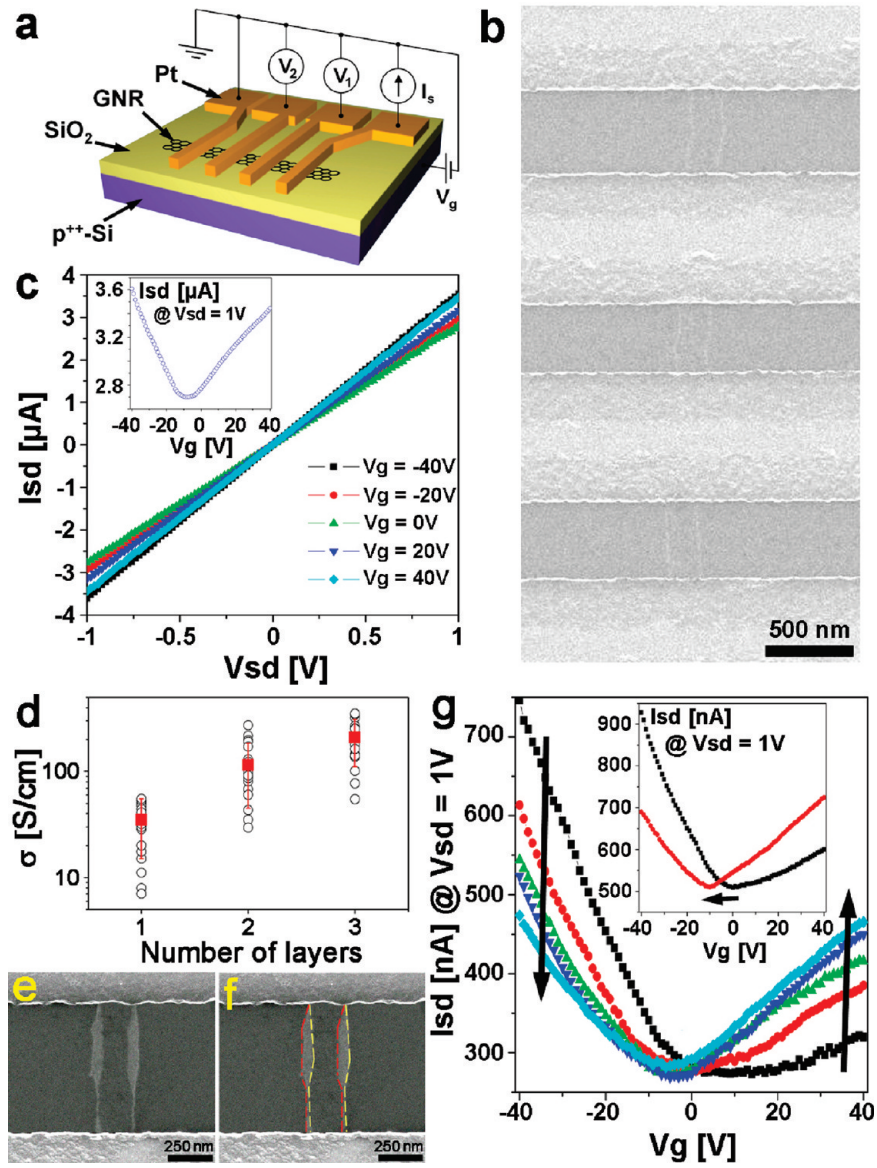

Figure 3. Electronic properties of GNRs reduced in Ar/H_2 at 900 °C for 1 h. (a) Schematic of the electrode arrangement on a GNR. (b) SEM image of a typical four-terminal device based on a monolayer nanoribbon. The bright horizontal strips are Pt electrodes and the faint orthogonal vertical line is the GNR. (c) Current−voltage ($I_{sd}-V_{sd}$) and transfer characteristics ($I_{sd}-V_g$) for a typical monolayer nanoribbon, recorded in four-terminal geometry. The source−drain distance is 500 nm and the width of the nanoribbon is 250 nm. (d) Logarithmic plot of the conductivity of the GNR devices *versus* the number of layers. Circles show the experimental data points (≥20 for each set of data); squares show the mean values. (e) SEM image of the electronic device based on hydrazine-reduced bilayer GNR. (f) The same SEM image as in panel e with the long edges of the different layers of the GNR shown by red and yellow dashed lines. The darker part in the middle of the GNR is the region where the top and bottom layers overlap. (g) The effect of chemical doping on the transfer characteristics of a monolayer GNR. The $I_{sd}-V_g$ curves were recorded a few minutes after pumping down the probe station chamber (■) and then at the pressure of 10^{-5} Torr after 12 h (red circle), 24 h (green triangle), 48 h (blue down triangle) and 72 h (turquoise diamond) of pumping. The inset shows the same effect for another device to better illustrate the shift of the neutrality point; the $I_{sd}-V_g$ curves were recorded at the pressure of 10^{-5} Torr after 1 h (■) and 48 h (red circle) of pumping. The measurements of panel g were done in two-probe geometry.

transfer characteristic curve became more symmetrical. This effect is completely reversible, since the device again shows p-type behavior after exposure to ambient conditions. This can be explained by adsorption of acceptor molecules, such as water and oxygen from the air, onto GNRs and their gradual desorption in vacuum.[42] Interestingly, this adsorbate-induced p-doping does not significantly alter the conductance at the neutrality point (minimum conductance point, V_{NP}), but V_{NP} shifts to more negative gate voltages (see Figure 3g and the inset therein) with the desorption of the acceptor molecules from the GNR surface; this is also in accord with previously reported data for exfoliated graphene.[40,42] The reversibility of the field effect suggests that the GNR devices may prove useful for making ultracompact gas sensors.

Recently it has been reported that two-terminal devices, where conductive carbon materials such as

monolayer graphene[43] or CVD-grown carbon[44,45] bridges two electrodes, can act as nonvolatile memories. These carbon layers first undergo electrical cleavage at a relatively high voltage, which results in a formation of a small (a few nm wide) crack across the carbon material; the conduction through this junction could be further modulated by applying certain electrical pulses.[43−45] Similar memory behavior was observed here for the GNR devices. The inset in Figure 4 shows that the device based on a N_2H_4-reduced few-layer (greater than three layers) GNR undergoes voltage-induced cleavage at ~8 V, which results in a formation of a crack across the nanoribbon and expansion of the upper graphene layers. Similar behavior was also observed for the two-terminal devices based on mono- and bilayer GNRs. Figure 4a shows that after that electrical cleavage event, the device has low conduction, which then abruptly increases at ~3.5 V and drops at 5 V; the forward and backward scan $I-V$ curves do not retrace each other as the device ends the double voltage sweep in a high-conduction state, exhibiting an ON/OFF ratio of $>10^6$. The high- and low-conduction states of device can be achieved through the voltage pulses in the "Write" and "Erase" regions, respectively; the potential working ranges of reading, writing, and erasing are indicated in Figure 4a. Figure 4b shows that the device could be subjected to 1000 "write−10 reads−erase−10 reads" cycles with no observable change in its performance, attesting to its cyclic endurance.

In summary, we have demonstrated a significantly streamlined fabrication process for GNR devices by using GNR solutions from unzipped carbon nanotubes. With the available shear-force alignment techniques, numerous graphene-based FETs, sensors, and memories can be fabricated on a single chip. This provides statistically relevant device assessments and insights into multilayering properties on conductance and the profound effects that atmospheric adsorbates have upon the transfer characteristics of graphene. The electrical conductivity of the reduced nanoribbons is much lower than that of the exfoliated graphene sheets but comparable or higher than for the reduced GO. Recent refinements in the synthetic procedure for unzipping nanotubes might provide GNRs with diminished oxidative damage and thereby enhanced electrical properties.[26]

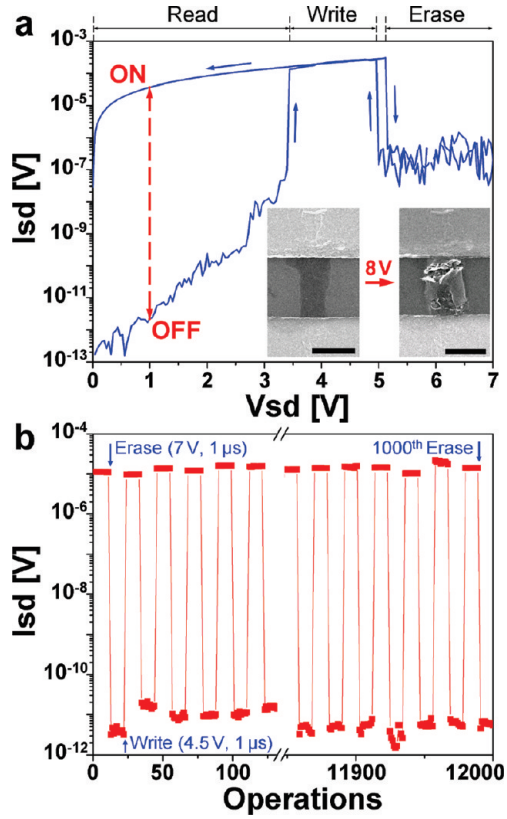

Figure 4. Two-terminal memory properties of a GNR device. (a) Logarithmic $I-V$ curve of the device based on a N_2H_4-reduced few-layer GNR after voltage induced cleavage of the carbon layer; the high- and low-conductance states of device can be achieved through voltage pulses in the "Write" and "Erase" regions, respectively. After writing or erasing, the state of the system is recorded in the "Read" voltage region. The inset shows SEM images of the device before and after electrical cleavage at ~8 V. The scale bars are 300 nm. (b) The cyclic endurance of the same device: pulses of +4.5 V and +7 V for 1 μs were used for writing and erasing, respectively. After each write/erase operation, the device current was consecutively read at +1 V 10 times. After 1000 cycles of write−read (10×)−erase−read (10×) operations, the memory showed no degradation of its ON/OFF current readings of $>10^6$.

EXPERIMENTAL SECTION

Synthesis of GONRs. MWCNTs were used as received from Mitsui & Co. (lot no. 05072001K28). The GONRs were prepared according to ref 24 where 5 g of $KMnO_4$ was used for each 1 g of MWCNTs. The concentration of $KMnO_4$ in H_2SO_4 was 0.5 wt %/vol (weight of $KMnO_4$ to volume of H_2SO_4) as originally reported.[14] **Caution:** *Do not exceed ~0.5 wt %/vol. It is reported that at much higher concentrations, namely 7 wt %/vol $KMnO_4$ in H_2SO_4, the mixture can explode upon heating.*[46]

Reduction of GONRs. The GONRs were dissolved in a water solution of 1 vol % conc. NH_4OH and 1 vol % $N_2H_4 \cdot H_2O$. ***Caution***: *Hydrazine is extremely corrosive and should be handled with care in an appropriate fume hood*. The solution was covered with a thin layer of silicon oil and then heated at 95 °C for 40−50 min. Further reduction was achieved by annealing the nanoribbons deposited onto Si/SiO_2 substrates in H_2/Ar (1:1, < 1 atm) atmosphere at 300−900 °C for 15−60 min.

Device Fabrication. For the alignment of GNRs on a Si/SiO_2 substrate, a droplet of a dilute solution of GNRs was put onto the substrate and spread over it by repeating unidirectional (away from the painter) strokes of a soft paintbrush while drying. After drying, the substrate was washed by a strong stream of DI water in the same direction as the brushing had occurred. Fabrication of graphene devices was performed by tracking individual GNRs on the surface of highly doped Si substrates, covered with 200-nm-thick dielectric SiO_2, by SEM (JEOL-6500 microscope), and followed by patterning of 20-nm-thick Pt contacts by standard electron beam lithography.

Sample Analysis. SEM imaging was performed on a JEOL-6500 field-emission microscope. AFM images were obtained with a Digital Instruments Nanoscope IIIa, operating in tapping mode, using Si tips *n*-doped with 1−10 Ωcm phosphorus (Veeco, MPP-11100-140) at a scan rate of 0.5 Hz and a resolution of 512 × 512. XPS was performed on a PHI Quantera SXM scanning X-ray microprobe. Raman spectroscopy was performed on a Renishaw Raman microscope using a 633-nm HeNe laser. The electrical transport properties were tested using a probe station (Desert Cryogenics TT-probe 6 system) under vacuum with chamber base pressure below 10^{-5} Torr. The IV data were collected by an Agilent 4155C semiconductor parameter analyzer.

Acknowledgment. Mitsui & Co., Ltd. generously donated the MWCNTs. This work was supported by the Air Force Research Laboratory through University Technology Corporation, 09-S568-064-01-C1, the Air Force Office of Scientific Research FA9550-09-1-0581, the Army Research Office through an SBIR with Privatran LLC and the Office of Naval Research MURI Graphene Program.

REFERENCES AND NOTES

1. Geim, A. K.; Novoselov, K. S. The Rise of Graphene. *Nat. Mater.* **2007**, *6*, 183–191.
2. Novoselov, K. S.; Geim, A. K.; Morozov, S. V.; Jiang, D.; Zhang, Y.; Dubonos, S. V.; Grigorieva, I. V.; Firsov, A. A. Electric Field Effect in Atomically Thin Carbon Films. *Science* **2004**, *306*, 666–669.
3. Novoselov, K. S.; Geim, A. K.; Morozov, S. V.; Jiang, D.; Katsnelson, M. I.; Grigorieva, I. V.; Dubonos, S. V.; Firsov, A. A. Two-Dimensional Gas of Massless Dirac Fermions in Graphene. *Nature* **2005**, *438*, 197–200.
4. Zhang, Y.; Tan, Y. W.; Stormer, H. L.; Kim, P. Experimental Observation of the Quantum Hall Effect and Berry's Phase in Graphene. *Nature* **2005**, *438*, 201–204.
5. Berger, C.; Song, Z.; Li, T.; Li, X.; Ogbazghi, A. Y.; Feng, R.; Dai, Z.; Marchenkov, A. N.; Conrad, E. H.; First, P. N.; de Heer, W. A. Ultrathin Epitaxial Graphite: 2D Electron Gas Properties and a Route toward Graphene-Based Nanoelectronics. *J. Phys. Chem. B* **2004**, *108*, 19912–19916.
6. Berger, C.; Song, Z.; Li, X.; Wu, X.; Brown, N.; Naud, C.; Mayou, D.; Li, T.; Hass, J.; Marchenkov, A. N.; *et al.* Electronic Confinement and Coherence in Patterned Epitaxial Graphene. *Science* **2006**, *312*, 1191–1196.
7. Morozov, S. V.; Novoselov, K. S.; Katsnelson, M. I.; Schedin, F.; Ponomarenko, L. A.; Jiang, D.; Geim, A. K. Strong Suppression of Weak Localization in Graphene. *Phys. Rev. Lett.* **2006**, *97*, 016801.
8. Chen, Z.; Lin, Y. M.; Rooks, M. J.; Avouris, P. Graphene Nano-ribbon Electronics. *Phys. E* **2007**, *40*, 228–232.
9. Han, M. Y.; Özyilmaz, B.; Zhang, Y.; Kim, P. Energy Band-Gap Engineering of Graphene Nanoribbons. *Phys. Rev. Lett.* **2007**, *98*, 206805.
10. Bolotin, K. I.; Sikes, K. J.; Jiang, Z.; Klima, M.; Fudenberg, G.; Hone, J.; Kim, P.; Stormer, H. L. Ultrahigh Electron Mobility in Suspended Graphene. *Solid State Commun.* **2008**, *146*, 351–355.
11. Lin, Y. M.; Jenkins, K. A.; Valdes-Garcia, A.; Small, J. P.; Farmer, D. B.; Avouris, P. Operation of Graphene Transistors at Gigahertz Frequencies. *Nano Lett.* **2009**, *9*, 422–426.
12. Kim, K. S.; Zhao, Y.; Jang, H.; Lee, S. Y.; Kim, J. M.; Kim, K. S.; Ahn, J. H.; Kim, P.; Choi, J. Y.; Hong, B. H. Large-Scale Pattern Growth of Graphene Films for Stretchable Transparent Electrodes. *Nature* **2009**, *457*, 706–710.
13. Li, X.; Cai, W.; An, J.; Kim, S.; Nah, J.; Yang, D.; Piner, R.; Velamakanni, A.; Jung, I.; Tutuc, E.; *et al.* Large-Area Synthesis of High-Quality and Uniform Graphene Films on Copper Foils. *Science* **2009**, *324*, 1312–1314.
14. Kosynkin, D. V.; Higginbotham, A. L.; Sinitskii, A.; Lomeda, J. R.; Dimiev, A.; Price, B. K.; Tour, J. M. Longitudinal Unzipping of Carbon Nanotubes to Form Graphene Nanoribbons. *Nature* **2009**, *458*, 872–876.
15. Sinitskii, A.; Fursina, A. A.; Kosynkin, D. V.; Higginbotham, A. L.; Natelson, D.; Tour, J. M. Electronic Transport in Monolayer Graphene Nanoribbons Produced by Chemical Unzipping of Carbon Nanotubes. *Appl. Phys. Lett.* **2009**, *95*, 253108.
16. Sinitskii, A.; Dimiev, A.; Corley, D. A.; Fursina, A. A.; Kosynkin, D. V.; Tour, J. M. Kinetics of Diazonium Functionalization of Chemically Converted Graphene Nanoribbons. *ACS Nano* **2010**, *4*, 1949–1954.
17. Sinitskii, A.; Kosynkin, D. V.; Dimiev, A.; Tour, J. M. Corrugation of Chemically Converted Graphene Monolayers on SiO_2. *ACS Nano* **2010**, *4*, 3095–3102.
18. Han, M. Y.; Brant, J. C.; Kim, P. Electron Transport in Disordered Graphene Nanoribbons. *Phys. Rev. Lett.* **2010**, *104*, 056801.
19. Bai, J.; Duan, X.; Huang, Y. Rational Fabrication of Graphene Nanoribbons Using a Nanowire Etch Mask. *Nano Lett.* **2009**, *9*, 2083–2087.
20. Liao, L.; Bai, J.; Cheng, R.; Lin, Y.; Jiang, S.; Huang, Y.; Duan, X. Top-Gated Graphene Nanoribbon Transistors with Ultrathin High-k Dielectrics. *Nano Lett.* **2010**, *10*, 1917–1921.
21. Li, X.; Wang, X.; Zhang, L.; Lee, S.; Dai, H. Chemically Derived, Ultrasmooth Graphene Nanoribbon Semiconductors. *Science* **2008**, *319*, 1229–1232.
22. Cai, J.; Ruffieux, P.; Jaafar, R.; Bieri, M.; Braun, T.; Blankenburg, S.; Muoth, M.; Seitsonen, A. P.; Saleh, M.; Feng, X.; *et al.* Atomically precise bottom-up fabrication of graphene nanoribbons. *Nature* **2010**, *466*, 470–473.
23. Cano-Márquez, A. G.; Rodríguez-Macías, F. J.; Campos-Delgado, J.; Espinosa-González, C. G.; Tristán-López, F.; Ramírez-González, D.; Cullen, D. A.; Smith, D. J.; Terrones, M.; Vega-Cantú, Y. I. Ex-MWNTs: Graphene Sheets and Ribbons Produced by Lithium Intercalation and Exfoliation of Carbon Nanotubes. *Nano Lett.* **2009**, *9*, 1527–1533.
24. Jiao, L; Zhang, L.; Wang, X.; Diankov, G.; Dai, H. Narrow Graphene Nanoribbons from Carbon Nanotubes. *Nature* **2009**, *458*, 877–880.
25. Elías, A. L.; Botello-Méndez, A. R.; Meneses-Rodríguez, D.; González, V. J.; Ramírez-González, D.; Ci, L.; Muñoz-Sandoval, E.; Ajayan, P. M.; Terrones, H.; Terrones, M. Longitudinal Cutting of Pure and Doped Carbon Nanotubes to Form Graphitic Nanoribbons Using Metal Clusters as Nanoscalpels. *Nano Lett.* **2010**, *10*, 366–372.
26. Higginbotham, A. L.; Kosynkin, D. V.; Sinitskii, A.; Sun, Z.; Tour, J. M. Lower-Defect Graphene Oxide Nanoribbons from Multiwalled Carbon Nanotubes. *ACS Nano* **2010**, *4*, 2059–2069.
27. Jiao, L.; Wang, X.; Diankov, G.; Wang, H.; Dai, H. Facile Synthesis of High-Quality Graphene Nanoribbons. *Nat. Nanotechnol.* **2010**, *5*, 321–325.
28. Schniepp, H. C.; Li, J. L.; McAllister, M. J.; Sai, H.; Herrera-Alonso, M.; Adamson, D. H.; Prud'homme, R. K.; Car, R.; Saville, D. A.; Aksay, I. A. Functionalized Single Graphene Sheets Derived from Splitting Graphite Oxide. *J. Phys. Chem. B* **2006**, *110*, 8535–8539.
29. Stankovich, S.; Dikin, D. A.; Piner, R. D.; Kohlhaas, K. A.; Kleinhammes, A.; Jia, Y.; Wu, Y.; Nguyen, S. T.; Ruoff, R. S. Synthesis of Graphene-Based Nanosheets *via* Chemical Reduction of Exfoliated Graphite Oxide. *Carbon* **2007**, *45*, 1558–1565.
30. Gilje, S.; Han, S.; Wang, M.; Wang, K. L.; Kaner, R. B. A Chemical Route to Graphene for Device Applications. *Nano Lett.* **2007**, *7*, 3394–3398.
31. Gómez-Navarro, C.; Weitz, R. T.; Bittner, A. M.; Scolari, M.; Mews, A.; Burghard, M.; Kern, K. Electronic Transport Properties of Individual Chemically Reduced Graphene Oxide Sheets. *Nano Lett.* **2007**, *7*, 3499–3503.
32. Tung, V. C.; Allen, M. J.; Yang, Y.; Kaner, R. B. High-Throughput Solution Processing of Large-Scale Graphene. *Nat. Nanotechnol.* **2009**, *4*, 25–29.
33. Eda, G.; Fanchini, G.; Chhowalla, M. Large-Area Ultrathin Films of Reduced Graphene Oxide as a Transparent and Flexible Electronic Material. *Nat. Nanotechnol.* **2009**, *3*, 270–274.

34. Stankovich, S.; Dikin, D. A.; Dommett, G. H. B.; Kohlhaas, K. M.; Zimney, E. J.; Stach, E. A.; Piner, R. D.; Nguyen, S. T.; Ruoff, R. S. Graphene-Based Composite Materials. *Nature* **2006**, *442*, 282–286.
35. Teweldebrhan, D.; Balandin, A. A. Modification of Graphene Properties due to Electron-Beam Irradiation. *Appl. Phys. Lett.* **2009**, *94*, 013101.
36. Ferrari, A. C.; Robertson, J. Interpretation of Raman Spectra of Disordered and Amorphous Carbon. *Phys. Rev. B* **2000**, *61*, 14095–14107.
37. Gupta, A. K.; Russin, T. J.; Gutiérrez, H. R.; Eklund, P. C. Probing Graphene Edges *via* Raman Scattering. *ASC Nano* **2009**, *3*, 45–52.
38. Malard, L. M.; Pimenta, M. A.; Dresselhaus, G.; Dresselhaus, M. S. Raman Spectroscopy in Graphene. *Phys. Reports* **2009**, *473*, 51–87.
39. Chen, J. H.; Jang, C.; Xiao, S.; Ishigami, M.; Fuhrer, M. S. Intrinsic and Extrinsic Performance Limits of Graphene Devices on SiO_2. *Nat. Nanotechnol.* **2008**, *3*, 206–209.
40. Chen, J. H.; Jang, C.; Adam, S.; Fuhrer, M. S.; Williams, E. D.; Ishigami, M. Charge-Impurity Scattering in Graphene. *Nat. Phys.* **2008**, *4*, 377–381.
41. Jung, I.; Dikin, D. A.; Piner, R. D.; Ruoff, R. S. Tunable Electrical Conductivity of Individual Graphene Oxide Sheets Reduced at "Low" Temperatures. *Nano Lett.* **2008**, *8*, 4283–4287.
42. Schedin, F.; Geim, A. K.; Morozov, S. V.; Hill, E. W.; Blake, P.; Katsnelson, M. I.; Novoselov, K. S. Detection of Individual Gas Molecules Adsorbed on Graphene. *Nat. Mater.* **2007**, *6*, 652–655.
43. Standley, B.; Bao, W.; Zhang, H.; Bruck, J.; Lau, C. N.; Bockrath, M. Graphene-Based Atomic-Scale Switches. *Nano Lett.* **2008**, *8*, 3345–3349.
44. Li, Y.; Sinitskii, A.; Tour, J. M. Electronic Two-Terminal Bistable Graphitic Memories. *Nat. Mater.* **2008**, *7*, 966–971.
45. Sinitskii, A.; Tour, J. M. Lithographic Graphitic Memories. *ACS Nano* **2009**, *3*, 2760–2766.
46. Olley, R. H.; Bassett, D. C. An Improved Permanganic Etchant For Polyolefines. *Polymer* **1982**, *23*, 1707–1710.